Article

A Photoelectrochemical Study of Hybrid Organic and Donor—Acceptor Dyes as Sensitizers for Dye-Sensitized Solar Cells

Jessica Barichello [1,2,*], Sara Gullace [3], Alberto Cusimano [1,4], Gaetano Di Marco [1], Fabio Matteocci [2] and Giuseppe Calogero [1,*]

1   IPCF-CNR, Istituto per i Processi Chimico-Fisici, Viale F. Stagno d'Alcontres 37, 98158 Messina, Italy; alberto.cusimano@unime.it (A.C.); dimarco@ipcf.cnr.it (G.D.M.)
2   CHOSE—Centre for Hybrid and Organic Solar Energy, Department of Electronic Engineering, University of Rome "Tor Vergata", 00133 Roma, Italy; fabio.matteocci@uniroma2.it
3   ISIS UMR 7006, CNRS, Université de Strasbourg, 8 Allée Gaspard Monge, 67000 Strasbourg, France; gullace@unistra.fr
4   Department of Chemical, Biological, Pharmaceutical and Environmental Sciences, University of Messina, Viale F. Stagno d'Alcontres 31, 98166 Messina, Italy
*   Correspondence: jessica.barichello@uniroma2.it (J.B.); giuseppe.calogero@cnr.it (G.C.); Tel.: +39-09039762 (J.B.); +39-09039762247 (G.C.)

Abstract: An investigation on the photoelectrochemical and sensitizing properties of two different hybrid organic dyes, anchored as sensitizers on mesoporous TiO_2, in Grätzel solar cells, is presented. Firstly, we studied the absorption properties of the C106 sensitizer, a Ru polypyridine complex, and of the Y123, an organic push and pull dye. In this work, we characterized these two dyes, employing two different electrolytes, with similar experimental condition and device parameters. From the J–V curves and IPCE photo action spectra, we performed an inedited bifacial study based on the comparison of their photovoltaic performances, exploiting several backgrounds (black or white). Among the obtained results from this study, we found the best bifaciality factor of 93% for C106 and the best power conversion efficiency of 12.8% for Y123. These results represent, concerning these two dyes and to the best of our knowledge, some of the highest values in literature.

Keywords: dye-sensitized solar cells; solar energy conversion; hybrid organic photovoltaics; bifacial solar devices

1. Introduction

Recent developments in the use of supramolecular self-assembly processes [1–4] have taken advantage of the synergistic employment of approaches and techniques that simultaneously investigate the structural organization and dynamic behavior at the nanoscale, thus offering a large variety of solutions in nanoscience, nano-engineering, and biotechnology [5–7]. The construction of multicomponent materials with controllable nanostructure and properties is fundamental to truly exploit the use of these functional materials in many potential applications [1,8–14]. Among these applications, the use of anchoring dyes as sensitizers for dye-sensitized solar cells (DSSCs) is based on the interaction and assembly of compounds with nanoparticles. DSSCs are a valid alternative to the more conventional Si-based PV technology concerning indoor application [8,15], owing to their potential low-cost production [16], easy fabrication, color tunability [17,18], and compatibility with esthetic design. In a typical DSSC, a dye-sensitized nano-crystalline TiO_2 on a conductive transparent glass absorbs the solar energy [19,20]. The photoexcitation of the dye molecules by photons promotes electrons' injection toward the conduction band (CB) of nano-crystalline TiO_2. The electrons are collected on the conductive glass of the working electrode (WE or anode) and flow through the external circuit and the load, then the electrons are reintroduced

into the cell by a counter electrode (CE) on the back, where they are transferred to an electrolytic solution placed between WE and CE. The role of the electrolyte is to regenerate the dye molecules in their ground state, ensuring the absorption of more photons [21]. In the past, many research efforts have been devoted to the mesoscopic DSSC since the pioneer demonstration of its feasibility as a low-cost photovoltaic technology [22]. Based on several material combinations, DSSC has achieved a respectable high efficiency [23] and a remarkable stability under the prolonged accelerating testing conditions [24–26].

In this work, we focused on two high-molar extinction coefficient (ε) sensitizers, belonging to the two main classes of dyes employed for DSSCs: ruthenium complexes and organic donor–π–acceptor (D–π–A) compounds. The first class is here represented by the C106 dye (cis-bis(isothiocyanato)(2,2′-bipyridyl-4,4′-dicarboxylato)(4,4′-bis(5-(hexylthio)thiophen-2-yl)-2,2′-bipyridyl) ruthenium(II)), whose structural formula is shown in Figure 1a. It is a ruthenium complex developed for high-efficiency DSSC [27], as a more efficient analogue of the well-known Z907 and C101 dyes. By introducing a sulfur atom of the bipyridyl (bpy) ligand inserted between hexyl and thiophene groups, it is possible to obtain a dye with a red shifted metal-to-ligand charge transfer (MLCT) band ensuring a higher molar extinction coefficient (ε). The second one to be investigated is the Y123 dye 3-{6-{4-[bis(2′,4′-dihexyloxybiphenyl-4-yl) amino-]phenyl}-4,4-dihexyl-cyclopenta-[2,1-b:3,4-b] dithiphene-2-yl}-2-cyanoacrylic acid. This organic dye is metal-free with a high molar extinction coefficient (ε) which makes it particularly interesting to use in thin films of TiO$_2$ [28]. It is characterized by a triarylamine donor framework which is able to efficiently absorb light and transfer the excited electron in the cyanoacrylic acid acceptor's orbitals, thanks to the extended π-conjugation ensured by the cyclopentadithiophene (CPDT) π-bridge. This organic dye belongs to the family of D35 dye [29]. The choice to compare in this work the C106 and Y123 dyes is due to the fact that they are considered as the most representative of the two categories, metal–Ru complexes and metal-free dye, respectively. Indeed, C106 has reached one of the highest power conversion efficiencies of 11.3% [21,27] and it demonstrated a robust stability when tested at 60 °C under light soaking. Y123, on the other hand, belongs to a group of new organic dyes (together with C218 and JF419) worthy of interest due to their large extinction coefficient with one –COOH group [30].

Despite several authors reporting in literature that the speed of electronic injection from the dye to the semiconductor is faster for ruthenium complexes such as C106 than for organic dyes such as Y123, the majority of organic dyes used for the development of high efficiencies DSSC belongs to the class of donor–π linker–acceptor dyes to which Y123 belongs. The difference in injection is probably due to the D–π–A structure of this organic dye and its coupling with the TiO$_2$ film. In the Y123 dye, the electron donor moiety is located in the triphenylamine unit, and the acceptor orbitals are on the cyanoacrylate group. Cyclopentadithiophene (CPDT) works as a π bridge between the donor and the acceptor for efficient electron conjugation. This bridge helps to increase the dipole moment and the improvement of the molar extinction coefficient of the dye molecule. However, due to the electron-rich nature of the triphenylamine donor moiety and the CPDT bridge, Y123 dye is also characterized by a charge injection voltage loss due to its high-lying LUMO energy level [31]. The relaxation of the excited state in the Y123 dye molecule competes with electronic injection in the TiO$_2$ conduction band. While for Ru-based dyes an ultrafast electron injection in the femtosecond time scale has been reported, the electronic injection for the Y123 dye is accurately monitored within 2 ps after excitation of the photoanode [20,21]. This also depends on the electrolyte: its role is to allow the closure of the circuit and thus allow the regeneration of the dye, a fundamental process to guarantee the cell continuity in operation. One of the most important parameters of this process is the speed, necessary both to avoid the degradation of the dye, and to prevent the back-injection phenomena and, in general, to maximize the delivered current.

Transparent or semitransparent electrodes of DSSC are a unique opportunity for use in building-integrated photovoltaics (BIPV) to exploit the light from the interior of the buildings as well as outside. The bifacial structure indeed uses the solar radiation

absorption on the front and rear surfaces of the solar cells [32–34]. Many researchers are active in this field with the aim to exploit this DSSC typical feature. Moreover, the bifacial factor may be used in tandem devices. To take advantage of the bifacial feature, the scattering layer must not be present in the DSSC cell. The scattering layer is an additional thin film (5 µm) on the semiconductor with nanoparticles larger than 20 nm, with the rule of scattering the light, thus boosting the optical absorption and ensuring adequate light trapping in the device [35,36].

The purpose of this work is the comparison and the understanding of dynamics that govern the photoelectrochemical properties of two different class of dyes: a ruthenium complex, C106, and an organic donor–π–acceptor compound, Y123, at the same conditions. We utilized two different electrolytes, the commercial (high-stability electrolyte) El-HSE and the homemade J8* [25], and we investigated the device's behavior when measuring from the front and from the rear side with the aim of confirming DSSC as valid candidate for the bifacial application in BIPV. Moreover, we emphasized the DSSC raising PCE ability when the albedo's effect is exploited, reaching PCE values of 12.8% and 10.3% with Y123 and C106, respectively. To the best of our knowledge, in literature, a PCE as high as 12.8% with Y123 dye has not been reported yet, since no one has studied the potential of Y123 under the albedo effect. Albedo is an expression of the ability of surfaces to reflect sunlight (heat from the sun). Light-colored surfaces return a large part of the sunrays back to the atmosphere (high albedo). Dark surfaces absorb the rays from the sun (low albedo). We reached one of highest bifaciality factors (BFs) in the literature, of 93%, with C106 dye on a white background, to the best of our knowledge. Concerning the PCE of the two dyes, we find an interesting trend change linked to the TiO_2 thickness. This is related to the different dyes' molecular structures.
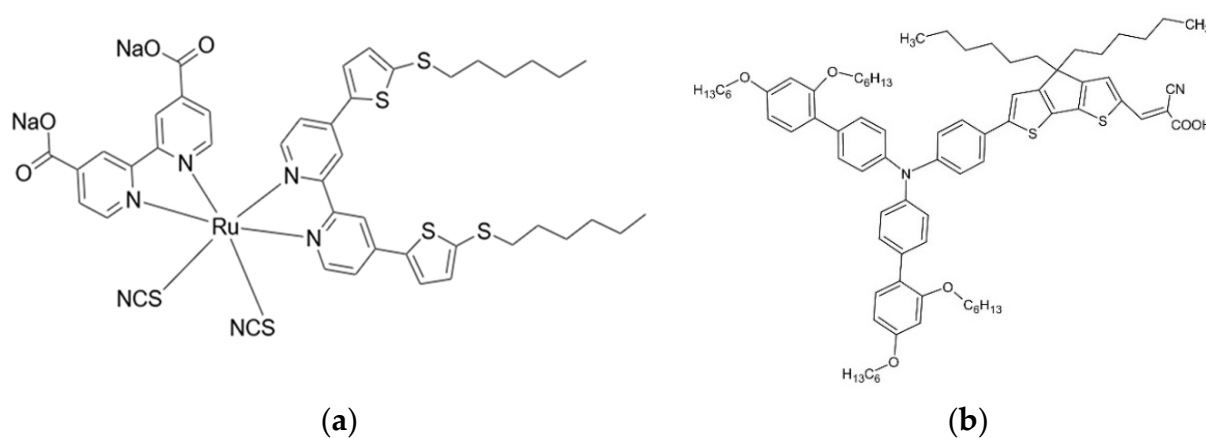
Figure 1. Molecular structure of (**a**) C106 dye and of (**b**) Y123 dye.

2. Materials and Methods

2.1. Cell's Fabrication Procedure

For the WE preparation, a conductive FTO (SnO_2: F; 2.2 mm TCO22-15) glass was firstly shaped as a square of 2.5 × 2.5 cm and cleaned with water, soap, acetone, and ethanol in an ultrasonic bath, 10 min each wash. Initially, electrodes were immersed for 30 min at 70 °C in a solution of $TiCl_4$ (844 µL in 100 mL of distilled H_2O; since the reaction is exothermic, the solution is obtained in an immersed beaker in an ice bath). This treatment mainly has two effects: increasing the resistance of the interaction between the FTO substrate and the TiO_2 film and blocking the charge recombination process between the electrons present on the semiconductor conduction band and the I_2 in the electrolyte. The suspension of TiO_2 plays a central role in the construction of the solar cell. Factors such as the size of the TiO_2 nanoparticles, the crystalline purity of the same, and the subsequent sintering steps are extremely important for the efficiency of the cell. In order to reduce the number of variables in the cell, we used a commercial TiO_2 suspension

for all devices: the DYESOL DSL 18NR-T (particle size of about 10–15 nm). The screen-printing technique was used in this study to deposit the TiO_2 paste [37]. This method allows obtaining TiO_2 films with precisely defined areas and constant thickness: the screen printing frame is made with a variable porosity polyester fabric, stretched on a frame of aluminum or iron. After blocking the conductive glass plate (15 cm × 4 cm) below the area of interest, several drops of TiO_2 paste are deposited on the frame and distributed through a doctor blade, maintaining, during this operation, a steady pressure. Finally, we proceed with a slow ramp sintering until 500 °C. The active area of the obtained photo anodes is approximately 0.181 cm^2. C106 (purity $\geq$ 85%) and Y123 (purity 99%) dyes were purchased from Dyesol and Dyenamo, respectively. WE were soaked in the dye solution (5 mM in terbutanol/acetonitrile in a 1:1 ratio) and the dye sensitization was carried out at room temperature for one night. Colored electrodes were washed with distilled water, then ethanol, and then dried. The homemade electrolytic solution J8* was prepared in acetonitrile (AN), a low-viscosity solvent (0.47 cp), and valeronitrile (whose viscosity is 0.78 cp) in a volumetric ratio of 85:15 v/v. In this way, a less volatile solution was obtained, resulting in a mixture with the following composition: LiI 0.1 M, I_2 0.05 M, tert-butyl pyridine (TBP) 0.5 M, and methyl-propyl imidazolium iodide (MPII) 0.6 M (J8*) [25]. High-stability electrolyte (El-HSE) was purchased from Great Solar; its composition is not quantitatively indicated, and it consists of a dissolved redox couple of triiodide/iodide in 3-methoxypropionitrile (3 MPN) solvent with inorganic iodide salt, organic iodide salt, and imidazole compound as additives as reported from the seller. Similar to WE, a conductive glass of FTO was cut, 2.5 × 2.5 cm, and cleaned to prepare the CE. The conductive surface was covered with a thin layer of catalyst. The latter performs the task of lowering the activation energy for the reduction of the I^-/I^{3-} torque. A few drops of hexachloroplatinic acid (H_2PtCl_6) solution were deposited on the substrates, arranged on a heating plate at 50 °C with the conductive surface facing upwards. The heat allows the evaporation of the solvent. Subsequently, the glasses were heated at 400 °C for 15 min, to eliminate hydrogen and chlorine, leaving only the metallic platinum. For sealing cells, a 25 μm thick Surlyn frame was placed on the conductive surface of the cathodes, previously drilled at an angle with diamond tips of 1 mm in diameter, which acted as a gasket. The photo-anode was placed on the cathode, making sure that the active area falls entirely within the edges of the frame. To obtain complete adhesion of the two conducting glasses, the entire system was placed inside a heated press at 120 °C for about 2 min. A small weight was then placed on the cell to avoid the formation of Surlyn bubbles due to thermal shock. Subsequently, the electrolyte solution was filled using a syringe that was introduced into the cathode hole, creating a vacuum and allowing the electrolytic mediator to enter, which was thus trapped inside the sandwich structure. The sealing procedure ended by applying a thin Surlyn film on the cathode hole and coupling the latter with another slide, fixed by heat.

2.2. Instrumental Section

A Perkin Elmer L20 spectrophotometer UV–Vis (range 180 nm–1100 nm) was utilized for absorption spectra. Current–voltage curves were obtained with a digital Keithley 236 multimeter connected to a PC and controlled by a homemade program. A LOT-Oriel solar simulator (Model LS0100-1000, 300 W Xe-Arc lamp, powered by LSN251 power supply equipped with AM 1.5 filter, 100 $mWcm^{-2}$) provided simulated sunlight irradiation. A Si-based pyranometer was used to calibrate incident irradiance. Incident photon-to-current conversion efficiency (IPCE or η) and relative photo-action spectra of sealed DSCs were measured by an IPCE station consisting of a 150 xenon light source (model ASB-XE, Spectral Products, Putnam, USA), a monochromator (model CM110, Spectral Products, Putnam, CT, USA) equipped with a slit set, a Si-calibrated detector (model 818-UV, Newport, Irvine, CA, USA), a picoammeter (model 6487, Keithley, Farnell®, Milan, Italy), and IPCE Solarena Software. TiO_2 layers' thickness were measured by using a DektakXT profilometer (Bruker, Arcore, Italy) equipped with a diamond-tipped stylus (radius of 2 μm) and selecting a

vertical scan range of 524 μm with 8.0 nm resolution, a programmed scan length of 6000 μm, and a stylus force of 1 mg.

3. Results and Discussion

3.1. Dyes' Optical Properties

The solutions of the two dyes are easily distinguished: one is red–orange (C106), while the other is yellow (Y123). One of the main requirements for a dye to be used as a sensitizer in DSSCs is to absorb light radiation in the visible region of the solar spectrum. Ethanol was chosen as solvent for both dyes since it is biodegradable and a natural product. The polar nature of ethanol ensures a suitable interaction with carboxyl polar functional groups and, on the other hand, its short alkyl chain favorably interacts also with the peripheral hydrocarbon chains in both compounds, C106 and Y123. In Figure 2a, the absorption spectra of C106 and Y123 dyes in ethanol are shown. Concerning the C106 spectrum, it exhibits in the UV region an intense sharp peak at 311 nm centered on ligand ($\pi \to \pi^*$), one large band (shoulder) from 349 to 398 nm, and another absorption maximum at 538 nm. The latest absorption bands can be assigned to singlet and triplet MLCT (metal to ligand charge transfer) transitions typical of the electronic charge transfer from the d metal orbitals to the π^* orbitals of the organic binders present in the C106. The organic dye Y123 (Figure 2a) is characterized by different optical properties due to its D–π–A structure: two main absorption peaks are found at 474 and 326 nm, with a hump at 260 nm, corresponding to the internal charge transfer (ICT) between the donor and the acceptor moieties and the $\pi \to \pi^*$ transition, respectively [38]. Moreover, it has been demonstrated that the flatness of the π-conjugated system, due to the presence of a melted cyclopentadithiophene structure, greatly increases the molar extinction coefficient at 532 nm (53×10^3 M^{-1}cm^{-1}), which is even greater than that reported in literature for C106 (18.7×10^3 M^{-1}cm^{-1} at 550 nm) [26]. The absorbance values reported in the spectra are in arbitrary units (a.u.) and cannot be quantitatively compared. The inset of Figure 2b shows two sensitized TiO$_2$ photoanodes (semiconductive layer thickness: 6–7 μm) with the C106 and Y123 dyes. The two photoanodes are visibly and uniformly colored, which indicates the dye has been efficiently adsorbed on the TiO$_2$ layer. From a visual observation, C106 photoanode appears darker than the sensitized one with Y123, even though the immersion time, the TiO$_2$ layer thickness, and the dyes solution concentrations were the same for the two different sensitizers. Figure 2b shows the absorption spectra of the sensitized photoanodes with C106 and Y123. In the C106 case, the first absorption bands, whose maximum were at 311 and 349 nm in solution, are hidden by the absorption spectrum of the TiO$_2$, which absorbs the light at higher energies (3.2 eV). On the other hand, the maxima of the third absorption band undergoes a slight bathochromic shift, from 398 to 401 nm and from 538 nm to 541 nm, respectively. This is probably a consequence of the interaction, between the carboxylic groups of the dye-anchoring moiety and the TiO$_2$, which stabilizes the dye in both the ground and the excited states. The TiO$_2$-anchoring group interaction also generates a red-shift of the ICT absorption band for Y123 from 474 nm to 485 nm when the dye is adsorbed on the semiconducting layer. Despite the highest molar extinction coefficient reported in literature for Y123, the Y123-sensitized photoanode exhibits lower intensity values than those of the corresponding C106 one. The most plausible explanation is that, given the same thickness and area, the density of absorbed C106 molecules on the photoanode is greater than those of Y123. This depends on the fact that the dye C106, which binds vertically to the TiO$_2$, with the 2,2'-bipyridyl (bpy) lying almost perpendicular to the TiO$_2$ surface, is less sterically hindered, while the Y123 structure, more rigid and planar, binds vertically with a greater steric hindrance due to the presence of the lateral-OC$_6$H$_{13}$ chains on the triphenylamine substituent. Moreover, since Y123 is prone to aggregation by π–π stacking due to its planar geometry, it is always used in association with disaggregating agents such as chenodeoxycholic acid (CDA): it has been demonstrated that CDA acts as a co-adsorbent on the TiO$_2$ surface, breaking of the π–π stacking thus avoiding the self-quenching of the dye molecules. Chandiran et al. demonstrated also that CDA as

a co-adsorbent with ruthenium C106 dye is not the best co-adsorber [39]. Moreover, by comparing the absorption spectra of two photoanodes with equal thickness, the organic dye λ max lies (485 nm) in the depression region between the two maxima of the Ru-based one (Figure 2b). The two spectra can be considered complementary, since the two compounds absorb throughout the region between 360 and 700 nm, thus suggesting their possible application in a "molecular cocktail" for more efficient panchromatic DSSCs.

(**a**)   (**b**)
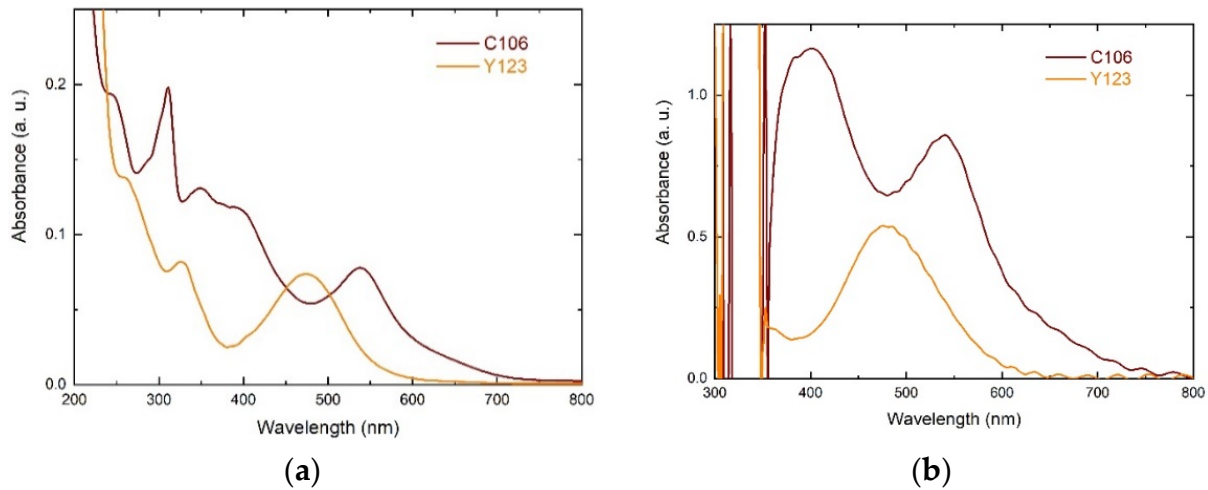
Figure 2. (**a**) Absorption spectra of dyes (C106, Y123) solution. (**b**) Absorption spectra of sensitized photoanodes with C106 and Y123 dyes (inset: photoanodes' image).

3.2. Bifacial Study on Two Different Electrolytes and Dyes

In this section, we investigate the two dyes' behavior with two different electrolytes, J8* and HSE, and, furthermore, we examine a bifacial DSSC application by irradiating the cell from the front side (glass–TiO$_2$–dye–electrolyte–platinum–glass*)* and from the rear side (glass–platinum–electrolyte–dye–TiO$_2$–glass) (Figure 3*)*. In Table 1, we summarize PV parameters of Y123 and C106 cells with two electrolytes application (HSE and homemade J8*), on black and white background (B and W*)*, and from the front and rear side.
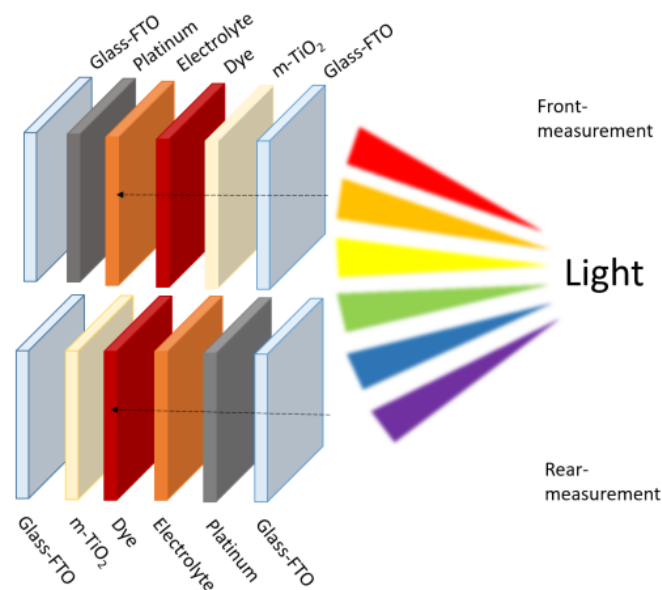
Figure 3. Graphic scheme of the front and rear lighting through the cell's layers.

3.2.1. The Electrolyte

All devices show better performances with electrolyte J8* than electrolyte HSE. J8*'s solvent is indeed composed by 85% (v:v) of acetonitrile, while HSE's solvent is methoxy propionitrile (3 MPN), as explained in Section 2. Acetonitrile is less viscous and more volatile than 3 MPN and this leads to a faster dye regeneration with the beneficial effect of Jsc increment in a device with J8* electrolyte. Moreover, J8* electrolyte also increases results due to less charge recombination: a faster dye regeneration due to a faster electrolyte diffusion means that the probability of dye's recombination for a back-electron-transfer phenomenon [40] is lower.

In Capasso et al. [41], a C106-based device with an iodine–iodide commercial electrolyte, high-performance electrolyte (HPE), similar to HSE, was developed. The main difference between HPE and HSE is the solvent: HPE employs acetonitrile, while HSE contains MPN. Despite the use of a more performant electrolyte, for reasons discussed above, the Pt-based/C106 device in Capasso et al. shows similar PCE (4.9%) to our work (4.8%) in similar condition (black background and thickness around 7–8 μm). This is due to the fact that Capasso et al. fabricated the DSSC device without the use of a blocking layer, as we made in this work. Considering our Pt-based C106 device, with J8* electrolyte, therefore, a similar solvent to HPE, we obtained 5.6% of PCE, a higher result due to the use of blocking layer in our device as discussed before. Concerning the Y123 dye, in Capasso et al. a similar procedure to ours was used to fabricate the cells. Indeed, the Y123-based device results in better performances: PCE in Capasso et al. is 9% while in this work is 4.92% in similar conditions (black background and thickness). In this case, the difference lies in the use of a cobalt-based electrolyte, more performant than an iodide/triiodide one. In a recent work that employs Y123 as a dye [30], with similar material and conditions to the ones of this work, a PCE of 5.3% was obtained. The slight difference between 4.92% (this work) and 5.3% [30] on a black background concerns the use of a scattering layer in the last work. Indeed, when our cell is measured in a white background (albedo effect) that works as a scattering layer, our result (5.6%) is in accordance with that in literature.

3.2.2. The Bifacial Factor

In the case of front-side irradiation, the electron path in the TiO$_2$ conduction band is shorter, and the hole path in the electrolyte, which span from the reduced dye to the platinum counter electrode, is longer in comparison to those for the case of rear-side irradiation. This effect can reduce the difference between the conversion efficiencies for front- and rear-side irradiation, resulting in high performance and enabling cost-effective application in large-scale solar power generation systems [42]. On the other hand, in the case of rear-side irradiation, the incident light is filtered by the iodide electrolyte [43], resulting in blocking the blue-light region and passing the red-light region. All rear-side measured devices show an increment in FF. From the rear side, fewer photons can reach the sensitized TiO$_2$, due to the platinum/electrolyte as middle layers that can absorb part of the photons. A minor number of photons reaching the sensitized TiO$_2$ leads to a more efficient electron injection and less charge recombination, which results in a FF increment.

All measured cell on a white background show better results in comparison to the respective measurement on a dark one. Indeed, the white background works as a scattering layer that can amplify the light effect, thus more photons can reach the device. Consequently, a current increment is observed on measured devices on white background. In the column "bifaciality factor" in Table 1, the ratio of each measured cell from the rear to the front side is reported for each dye, electrolyte, and background. With a black background, the BF is lower than the respective cell in the white one. A maximum BF of 93% has been obtained with C106 dye, J8* electrolyte, and a white background.

Considering the results in Table 1, it is possible to notice that BF is influenced by the electrolyte and by the dye. J8-electrolyte-based devices have a BF higher than HSE-based ones, and this depends on the different viscosity of the employed solvents. As discussed previously, J8 solvent allows a faster regeneration of the redox couple, and this brings

better performances in the rear side also. Analyzing BF differences for both electrolytes, we notice that the most influenced parameter is the current density; indeed, considering HSE-C106 device from rear to front, the current doubles (from 6.42 to 11.99 mA/cm^2), different to the case of J8-C106, where Jsc increment is less evident (from 9.62 to 13.94 mA/cm^2). A BF of 93% was achieved due to the exploitation of the albedo effect with C106 on a white background: more scattered photons and less differences between Jsc from rear to front (from 19.34 to 21.07 mA/cm^2). It is worth highlighting that exploiting the albedo effect, a standard DSSC cell reached the bifaciality factor of 93%, and this is mandatory to understand the great potential of this technology when used as BIPV in windows or indoor environment, even with different angle inclinations.

C106 has a higher BF than Y123 (and therefore less differences between front- and rear-side measurements) and it is possible to find the explanation when observing their absorbance spectra (Figure 2b). A sensitized C106 dye in a TiO$_2$ surface shows two maximum peaks at 401 and 541 nm. Iodine/iodide electrolyte absorbs from 300 to 400 nm [44]; therefore, in the rear side, when the electrolyte first filters the light, this cannot block the C106 excitation in the second band at 540 nm. On the other hand, Y123 has one absorption band from 400 to 500 nm, partially influenced by the filtered light from the electrolyte; from the rear side, this probably leads to higher PCE differences from front to rear for Y123 dye than for C106 dye.

3.2.3. The Incident Photon to Current Efficiency

In Figure 4, the IPCE graph of C106 (Figure 4a) and of Y123 (Figure 4b) dyes with J8* and HSE electrolytes, rear and front side, respectively, are shown. As previously mentioned, the platinum/electrolyte influence in rear-side measurement is noticeable with both dyes and both electrolytes (Figure 4a,b). Indeed, rear-side measurements show a less photons absorbance from 450 to 550 nm in comparison to the front side (for C106, Y123, HSE, and J8* electrolytes) where photons directly reach the sensitized TiO$_2$ without crossing the electrolyte solution first. The C106-based device obtained higher PCE than Y123-based ones, consistently with absorption spectra of Figure 2b, where C106 absorbance is greater than Y123, although the latter has an higher molar extinction coefficient. C106 absorption spectra show a superior photon capture, as confirmed from electrical parameters that demonstrate C106's better performances, in terms of PCE, compared to Y123 for all measurement situations (Table 1).

Table 1. PV parameters.

Electrolyte	Sample *	PCE (%)	Bifaciality Factor (%)	Jsc (mA/cm^2)	Voc (Volt)	FF (%)	IPCE (%)
J8*	B_C106_Front	5.61	75	13.94	0.66	61	100
	B_C106_Rear	4.19		9.62	0.66	66	75
	W_C106_Front	8.11	93	21.07	0.7	55	/
	W_C106_Rear	7.58		19.34	0.7	56	/
	B_Y123_Front	4.92	42	9.78	0.7	72	85
	B_Y123_Rear	2.07		3.93	0.7	75	40
	W_Y123_Front	6.48	72	13.24	0.71	69	/
	W_Y123_Rear	4.67		9.15	0.71	72	/
HSE	B_C106_Front	4.83	61	11.99	0.66	61	84
	B_C106_Rear	2.95		6.42	0.66	69	53
	W_C106_Front	6.74	84	16.8	0.68	59	/
	W_C106_Rear	5.63		13.76	0.66	62	/
	B_Y123_Front	3.77	58	8.52	0.66	67	75
	B_Y123_Rear	2.17		4.63	0.67	70	34
	W_Y123_Front	5.26	82	12.28	0.68	63	/
	W_Y123_Rear	4.34		9.64	0.68	66	/

* B: black background; W: white background. A mask was applied on the device as a frame for the active area. TiO$_2$ film thickness is 7 µm.
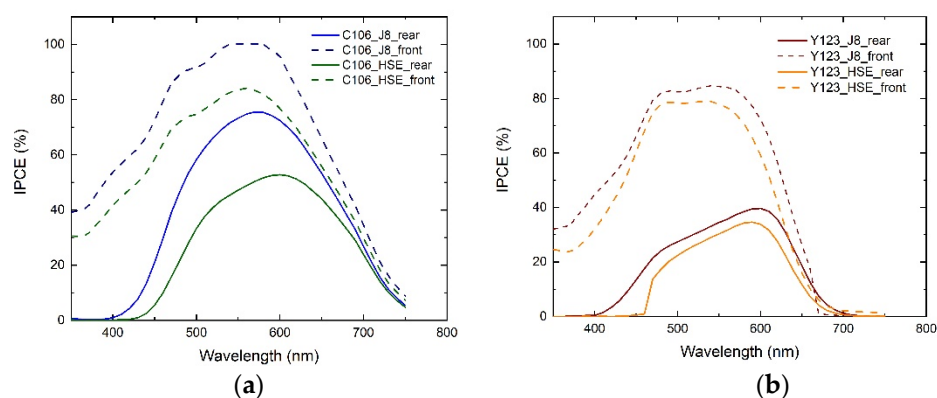
Figure 4. IPCE spectra of C106 and Y123 device. Cell were measured in a black background: (**a**) C106 device with J8* and HSE electrolytes, front and rear side; (**b**) Y123 device with J8* and HSE electrolytes, front and rear side.

3.3. TiO$_2$ Thickness Effect

Figure 5 shows the J–V curves of C106 and Y123 devices with an increased TiO$_2$ film thickness (12 µm) in comparison to devices reported in Table 1 (7 µm). The J8* electrolyte has been used as it is more performant than HSE. With a thicker TiO$_2$ layer (12 µm), the PCE of C106 and Y123 devices have similar results, unlike a thinner layer (7 µm), as reported in Table 1, where C106 is significantly more performant. As discussed previously, C106 has a greater absorbance in comparison to Y123 (Figure 2b) and saturates the light absorption at 7 µm thickness, as observed in IPCE spectra (Figure 4a). Comparing data of Table 1 (7 µm) and Table 2 (12 µm), considering the same measurement condition (black background) and electrolyte, J8*, C106 dye shows an almost unchanged PCE (5.6% with 7 µm and 5.9% with 12 µm). Indeed, Y123, at the same precedent condition, shows a PCE boost, respectively, to the TiO$_2$ increment from 4.9% to 6.3%, mainly due to the Jsc (from 9.8 to 12.5 mA/cm^2). This phenomenon is due to the C106 self-absorption processes which occur with increasing thickness [45]. Differently, Y123 has a lower absorbance, and it is not influenced by this effect at 12 µm. Figure 5 shows the J–V curves relative to the measurements made on the same cells subjected to irradiation without a mask and with a white background, which represent the working conditions in an outdoor environment where one obviously tries to maximize the collection of sunlight. One of the main advantages of the Grätzel cells (DSSCs), compared to the traditional silicon-based solar cells, is found in their ability to be passed through by parts of solar radiation, therefore it is possible to use the "albedo effect": the diffused and reflected light by the ground they are laying. This is obviously not possible for silicon solar cells or, in general, for opaque ones. While C106 and Y123 devices measured with a mask in a black background obtained similar results in terms of PCE (5.9 for Y123 and 6.34 for C106), the same devices measured without a mask and on a white background show significant differences in terms of PCE (12.78 for Y123 and 10.28 for C106), mainly due to the density current (26.68 mA/cm^2 for Y123 and 22.60 mA/cm^2 for C106) (Table 2 and Figure 5). Since the Y123 dye absorbs less radiation than C106 (see Figure 2b, more residual light is impinging on the white background and can be reflected to re-cross the solar cell: a greater albedo effect can explain both the higher photocurrent and efficiency found for the Y123 DSSC compared to the C106 one.
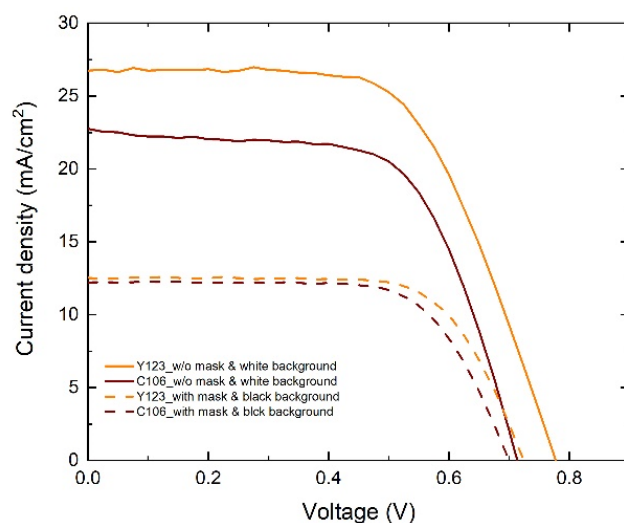
Figure 5. J–V of C106 and Y123 devices (TiO$_2$ film thickness of 11.6 μm) on white and black background.

Table 2. Electrical parameters of J–V curves of C106 and Y123 devices (TiO$_2$ film thickness of 11.6 μm) on white and black background.

Sample	PCE (%)	Jsc (mA/cm^2)	Voc (Volt)	FF (%)
B_C106	5.90	12.20	0.72	61
W_C106	10.28	22.69	0.71	63
B_Y123	6.34	12.50	0.70	70
W_Y123	12.78	26.68	0.77	62

4. Conclusions

In this work, we first investigated the differences between the optical properties of two dyes: a ruthenium complex, C106, and an organic donor–π–acceptor compound, Y123. The analysis of the absorption spectra shows that the Y123 photo-anode exhibits an absorption maximum peak at 485 nm, which, despite the highest molar extinction coefficient of this dye, has lower intensity values than those of the C106 photo-anode (401 and 541 nm). This evidence finds an explanation in the fact that C106 binds vertically to the TiO$_2$, with the bpy lying almost perpendicular to the TiO$_2$ surface, resulting as less sterically hindered, while the Y123 structure, more rigid and planar, binds vertically with a greater steric hindrance due to the presence of the lateral-OC$_6$H$_{13}$ chains on the triphenylamine substituent. Moreover, we studied dyes' behavior when they were employed as sensitizers in a DSSC, focusing on several operating conditions, such as electrolyte composition, thickness of anode, and illumination environment. For this purpose, we performed measurements illuminating the cells both from the front and rear sides, discussing from a scientific point of view the change in electrical parameters. We achieved one of the highest bifaciality factors (BF) in the literature, of 93%, with C106 dye on a white background, to the best of our knowledge. This is important to highlight the great potential of a standard DSSC device when exploited in BIPV or in an indoor environment when the albedo effect can be present. We noticed an interesting effect concerning the devices' performances related to the TiO$_2$ thickness. C106 dye has a great absorption capacity, as seen from absorbance spectra, and its PCE trend is not significantly influenced by TiO$_2$ thickness. On the other hand, the organic dye, Y123, with a lower absorbance, is positively affected by TiO$_2$ thickness, increasing the PCE. Furthermore, when the albedo's effect was exploited, Y123 and C106 achieved PCE values of 12.8% and 10.3%, respectively.

References

1. Li, Q. *Functional Organic and Hybrid Nanostructured Materials: Fabrication, Properties, and Applications*; Wiley-VCH Verlag GmbH & Co. KGaA: Weinheim, Germany, 2018.

2. Bonaccorsi, L.; Calandra, P.; Kiselev, M.A.; Amenitsch, H.; Proverbio, E.; Lombardo, D. Self-assembly in poly(dimethylsiloxane)-poly(ethylene oxide) block copolymer template directed synthesis of linde type A zeolite. *Langmuir* **2013**, *29*, 7079–7086. [CrossRef] [PubMed]

3. Bonaccorsi, L.; Calandra, P.; Amenitsch, H.; Proverbio, E.; Lombardo, D. Growth of fractal aggregates during template directed SAPO-34 zeolite formation. *Microporous Mesoporous Mater.* **2013**, *167*, 3–9. [CrossRef]

4. Turetta, N.; Stoeckel, M.; de Oliveira, R.F.; Devaux, F.; Greco, A.; Cendra, C.; Gullace, S.; Gicevičius, M.; Chattopadhyay, B.; Liu, J.; et al. High-Performance Humidity Sensing in π-Conjugated Molecular Assemblies through the Engineering of Electron/Proton Transport and Device Interfaces. *Am. Chem. Soc.* **2022**, *6*, 2546–2555. [CrossRef] [PubMed]

5. Chen, C.; Wylie, R.A.L.; Klinger, D.; Connal, L.A. Shape Control of Soft Nanoparticles and Their Assemblies. *Chem. Mater.* **2017**, *29*, 1918–1945. [CrossRef]

6. Lombardo, D.; Calandra, P.; Magazù, S.; Wanderlingh, U.; Barreca, D. Soft nanoparticles charge expression within lipid membranes: The case of amino terminated dendrimers in bilayers vesicles. *Colloids Surf. B Biointerfaces* **2018**, *170*, 609–616. [CrossRef]

7. Lombardo, D.; Munaò, G.; Calandra, P.; Pasqua, L.; Caccamo, M.T. Evidence of pre-micellar aggregates in aqueous solution of amphiphilic PDMS–PEO block copolymer. *Phys. Chem. Chem. Phys.* **2019**, *21*, 11983–11991. [CrossRef]

8. Freitag, M.; Teuscher, J.; Saygili, Y.; Zhang, X.; Giordano, F.; Liska, P.; Hua, J.; Zakeeruddin, S.M.; Moser, J.-E.; Grätzel, M.; et al. Dye-sensitized solar cells for efficient power generation under ambient lighting. *Nat. Photon.* **2017**, *11*, 372–378. [CrossRef]

9. Gullace, S.; Montes-García, V.; Martín, V.; Larios, D.; Consolaro, V.G.; Obelleiro, F.; Calogero, G.; Casalini, S.; Samorì, P. Universal Fabrication of Highly Efficient Plasmonic Thin-Films for Label-Free SERS Detection. *Small* **2021**, *17*, 2100755. [CrossRef]

10. Urbanos, F.J.; Gullace, S.; Samorì, P. Field-effect-transistor-based ion sensors: Ultrasensitive mercury(II) detection via healing MoS2 defects. *Nanoscale* **2021**, *13*, 19682. [CrossRef]

11. Mathew, R.J.; Lee, C.; Tseng, C.; Chand, P.K.; Huang, Y.; Chen, H.; Ho, K.; Anbalagan, A.; Lee, C.; Chen, Y.-T. Stoichiometry-Controlled MoxW1–xTe2 Nanowhiskers: A Novel Electrocatalyst for Pt-Free Dye-Sensitized Solar Cells. *ACS Appl. Mater. Interfaces* **2020**, *12*, 34815–34824. [CrossRef]

12. Karuppuchamyc, S.; Vijayaraghavan, S.; Gopalraman, A. High efficiency dye-sensitized solar cells with VOC–JSC trade off eradication by interfacial engineering of the photoanode|electrolyte interface. *RSC Adv.* **2019**, *9*, 40292–40300.

13. Calabrò, E.; Matteocci, F.; Paci, B.; Cina, L.; Vesce, L.; Barichello, J.; Generosi, A.; Reale, A.; di Carlo, A. Easy strategy to enhance thermal stability of planar PSCs by perovskite defect passivation and low-temperature carbon-based electrode. *ACS Appl. Mater. Interfaces* **2020**, *12*, 32536–32547. [CrossRef] [PubMed]

14. Barichello, J.; Vesce, L.; Matteocci, F.; Lamanna, E.; di Carlo, A. The effect of water in Carbon-Perovskite Solar Cells with optimized alumina spacer. *Sol. Energy Mater. Sol. Cells* **2019**, *197*, 76–83. [CrossRef]

15. Devadiga, D.; Selvakumar, M.; Shetty, P.; Santosh, M.S. Dye-Sensitized Solar Cell for Indoor Applications: A Mini-Review. *J. Electron. Mater.* **2021**, *50*, 3187–3206. [CrossRef]

16. Minicante, S.A.; Ambrosi, E.; Back, M.; Barichello, J.; Cattaruzza, E.; Gonella, F.; Scantamburlo, E.; Trave, E. Development of an eco-protocol for seaweed chlorophylls extraction and possible applications in dye sensitized solar cells. *J. Phys. D Appl. Phys.* **2016**, *49*, 295601. [CrossRef]

17. Calogero, G.; Citro, I.; Sebastianella, G.C.; di Marco, G.; Diniz, A.M.; Parola, A.J.; Pina, F. A Photoelectrochemical Study of Bioinspired 2-Styryl-1-Benzopyrylium Cations on TiO$_2$ Nanoparticle Layer for Application in Dye-Sensitized Solar Cells. *Materials* **2019**, *12*, 4060. [CrossRef] [PubMed]

18. Borella, L.; Vesce, L.; Mariani, P.; Barichello, J.; di Carlo, A.; Trivellin, N.; Sforza, E. Spectral Changes by Dye Sensitized Solar Modules Influence the Pigment Composition and Productivity of Arthrospira maxima and Increase the Overall Energy Efficiency. *Adv. Sustain. Syst.* **2022**, 2100346. [CrossRef]

19. O'Reagan, B.; Grätzel, M. A low-cost, high-efficiency Solar-Cell based on Dye-Sensitized Colloidal TiO_2 films. *Nature* **1991**, *353*, 737–740. [CrossRef]

20. Hagfeldt, A.; Boschloo, G.; Sun, L.; Kloo, L.; Pettersson, H. Dye Sensitized Solar Cell. *Chem. Rev.* **2010**, *110*, 6595–6663. [CrossRef]

21. Calogero, G.; Bartolotta, A.; di Marco, G.; di Carlo, A.; Bonaccorso, F. Vegetable-based dye-sensitized solar cells. *Chem. Soc. Rev.* **2015**, *44*, 3244. [CrossRef]

22. Bellani, S.; Bartolotta, A.; Agresti, A.; Calogero, G.; Grancini, G.; di Carlo, A.; Kymakis, E.; Bonaccorso, F. Solution-processed two-dimensional materials for next-generation photovoltaics. *Chem. Soc. Rev.* **2021**, *50*, 11870–11965. [CrossRef]

23. Kakiage, K.; Aoyama, Y.; Yano, T.; Oya, K.; Fujisawa, J.; Hanaya, M. Highly-efficient dye-sensitized solar cells with collaborative sensitization by silyl-anchor and carboxy-anchor dyes. *Chem. Commun.* **2015**, *51*, 15894–15897. [CrossRef]

24. Kato, N.; Higuchi, K.; Tanaka, H.; Nakajima, J.; Sano, T.; Toyoda, T. Improvement in long-term stability of dye-sensitized solar cell for outdoor use. *Sol. Energy Mater. Sol. Cells* **2011**, *95*, 301–305. [CrossRef]

25. Calogero, G.; Barichello, J.; Citro, I.; Mariani, P.; Vesce, L.; Bartolotta, A.; di Carlo, A.; di Marco, G. Photoelectrochemical and spectrophotometric studies on dye-sensitized solar cells (DSCs) and stable modules (DSCMs) based on natural apocarotenoids pigments. *Dye. Pigment.* **2018**, *155*, 75–83. [CrossRef]

26. Barichello, J.; Vesce, L.; Mariani, P.; Leonardi, E.; Braglia, R.; di Carlo, A.; Canini, A.; Reale, A. Stable Semi-Transparent Dye-Sensitized Solar Modules and Panels for Greenhouse Application. *Energies* **2021**, *14*, 6393. [CrossRef]

27. Cao, Y.; Bai, Y.; Yu, Q.; Cheng, Y.; Liu, S.; Shi, D.; Gao, F.; Wang, P. Dye-Sensitized Solar Cells with a High Absorptivity Ruthenium Sensitizer Featuring a 2-(Hexylthio)thiophene Conjugated Bipyridine. *J. Phys. Chem. C* **2009**, *113*, 6290–6297. [CrossRef]

28. Perganti, D.; Giannouri, M.; Kontos, A.G.; Falaras, P. Cost-efficient platinum-free DSCs using colloidal graphite counterelectrodes combined with D35 organic dye and cobalt (II/III) redox Couple. *Electrochim. Acta* **2017**, *232*, 517–527. [CrossRef]

29. Yella, A.; Mathew, S.; Aghazada, S.; Comte, P.; Gratzel, M.; Khaja, M.; Nazeeruddin. Dye-sensitized solar cells using cobalt electrolytes: The influence of porosity and pore size to achieve high-efficiency. *J. Mater. Chem. C* **2017**, *5*, 2833. [CrossRef]

30. Chandrasekhar, P.S.; Parashar, P.K.; Swami, S.K.; Komarala, V.K.; Dutta, V. Enhancement of Y123 dye-sensitized solar cells performance using plasmonic gold nanorods. *Phys. Chem. Chem. Phys.* **2018**, *20*, 9651–9658. [CrossRef]

31. Zhang, W.; Wu, Y.; Bahng, H.W.; Cao, Y.; Yi, C.; Saygili, Y.; Luo, J.; Liu, Y.; Kavan, L.; Moser, J.E.; et al. Comprehensive control of voltage loss enables 11.7% efficient solid-state dye-sensitized solar cells. *Energy Environ. Sci.* **2018**, *11*, 1779. [CrossRef]

32. Putri, T.E.; Chawarambwa, F.L.; Son, M.K.; Attri, P.; Kamataki, K.; Itagaki, N.; Koga, K.; Shiratani, M. Performance Characteristics of Bifacial Dye-Sensitized Solar Cells with a V-Shaped Low-Concentrating Light System. *ACS Appl. Energy Mater.* **2021**, *4*, 13410–13414. [CrossRef]

33. Xu, T.; Kong, D.; Tang, H.; Qin, X.; Li, X.; Gurung, A.; Kou, K.; Chen, L.; Qiao, Q.; Huang, W. Transparent MoS2/PEDOT Composite Counter Electrodes for Bifacial Dye-Sensitized Solar Cells. *ACS Omega*, 2020; 5, 8687–8696.

34. Xia, J.; Wang, Q.; Xu, Q.; Yu, R.; Chen, L.; Jiao, J.; Fana, S.; Wu, H. High efficiency bifacial quasi-solid-state dye-sensitized solar cell based on $CoSe_2$ nanorod counter electrode. *Appl. Surf. Sci.* **2020**, *530*, 147238. [CrossRef]

35. Hore, S.; Vetter, C.; Kern, R.; Smit, H.; Hinsch, A. Influence of scattering layers on efficiency of dye-sensitized solar cells. *Sol. Energy Mater. Sol. Cells* **2006**, *90*, 1176–1188. [CrossRef]

36. Barichello, J.; Mariani, P.; Matteocci, F.; Vesce, L.; Reale, A.; Di Carlo, A.; Lanza, M.; Di Marco, G.; Polizzi, S.; Calogero, G. The Golden Fig: A Plasmonic Effect Study of Organic-Based Solar Cells. *Nanomaterials* **2022**, *12*, 267. [CrossRef] [PubMed]

37. Mariani, P.; Vesce, L.; di Carlo, A. The role of printing techniques for large-area dye sensitized solar cells. *Semicond. Sci. Technol.* **2015**, *30*, 104003. [CrossRef]

38. Chaitanya, K.; Ju, X.; Heron, B.M. Can elongation of the p-system in triarylamine derived sensitizers with either benzothiadiazole and/or ortho-fluorophenyl moieties enrich their light harvesting efficiency? –A theoretical study. *RSC Adv.* **2015**, *5*, 3978–3998. [CrossRef]

39. Kumar Chandiran, A.; Zakeeruddin, S.M.; Humphry-Baker, R.; Khaja Nazeeruddin, M.; Grätzel, M.; Sauvage, F. Investigation on the Interface Modification of TiO_2 Surfaces by Functional Co-Adsorbents for High-Efficiency Dye-Sensitized Solar Cells. *ChemPhysChem* **2017**, *18*, 2724–2731. [CrossRef]

40. Listorti, A.; O'Regan, B.; Durrant, J.R. Electron Transfer Dynamics in Dye-Sensitized Solar Cells. *Chem. Mater.* **2011**, *23*, 3381–3399. [CrossRef]

41. Capasso, A.; Bellani, S.; Palma, A.L.; Najafi, L.; Del Rio Castillo, A.E.; Curreli, N.; Cinà, L.; Miseikis, V.; Coletti, C.; Calogero, G.; et al. CVD-graphene/graphene flakes dual-films as advanced DSSC counter electrodes. *2D Mater.* **2019**, *6*, 035007. [CrossRef]

42. Venkatesan, S.; Lin, W.H.; Teng, H.; Le, Y.H. High-Efficiency Bifacial Dye-Sensitized Solar Cells for Application under Indoor Light Conditions. *ACS Appl. Mater. Interfaces* **2019**, *11*, 42780–42789. [CrossRef]

43. Kang, M.G.; Park, N.G.; Ryu, K.S.; Chang, S.H.; Kim, K.J. A 4.2% efficient flexible dye-sensitized TiO_2 solar cell using stainless steel substrate. *Sol. Energy Mater. Sol. Cells* **2006**, *90*, 574–581. [CrossRef]

44. Shaban, S.; Roy, P.; Vats, A.K.; Pandey, S.S. Bifacial dye-sensitized solar cells utilizing green-colored NIR sensitive unsymmetrical squaraine dye. *Jpn. J. Appl. Phys.* **2022**, *61*, SB1005. [CrossRef]

45. Kalyanasundaram, K. Chapter 8, How to make high-efficiency dye-sensitized solar cells. In *Dye-Sensitized Solar Cell*, 1st ed.; EPFL Press Taylor e Francis Group: Lausanne, Switzerland, 2010; pp. 263–264.